BIOCHEMISTRY
including biophysical chemistry & molecular biology

Article

pubs.acs.org/biochemistry

Quantum and Classical Simulations of Orotidine Monophosphate Decarboxylase: Support for a Direct Decarboxylation Mechanism

Alexandra Vardi-Kilshtain, Dvir Doron, and Dan Thomas Major*

Department of Chemistry and the Lise Meitner-Minerva Center of Computational Quantum Chemistry, Bar-Ilan University, Ramat-Gan 52900, Israel

Supporting Information

ABSTRACT: Orotidine 5′-monophosphate (OMP) decarboxylase (ODCase) catalyzes the decarboxylation of OMP to uridine 5′-monophosphate (UMP). Numerous studies of this reaction have suggested a plethora of mechanisms including covalent addition, ylide or carbene formation, and concerted or stepwise protonation. Recent experiments and simulations present strong evidence for a direct decarboxylation mechanism, although direct comparison between experiment and theory is still lacking. In the current work we present hybrid quantum mechanics−molecular mechanics simulations that address the detailed decarboxylation mechanisms for OMP and 5-fluoro-OMP by ODCase. Multidimensional potentials of mean force are computed as functions of structural progress coordinates for the *Methanobacterium thermoautotrophicum* ODCase reaction: the decarboxylation reaction coordinate, an orbital rehybridization coordinate, and the proton transfer coordinate between Lys72 and the substrate. The computed free energy profiles are in accord with the available experimental data. To facilitate further direct comparison with experiment, we compute the kinetic isotope effects (KIEs) for the enzyme-catalyzed reactions using a mass-perturbation-based path-integral method. The computed KIE provide further support for a direct decarboxylation mechanism. In agreement with experiment, the data suggest a role for Lys72 in stabilizing the transition state in the catalysis of OMP and, to a somewhat lesser extent, in 5-fluoro-OMP.

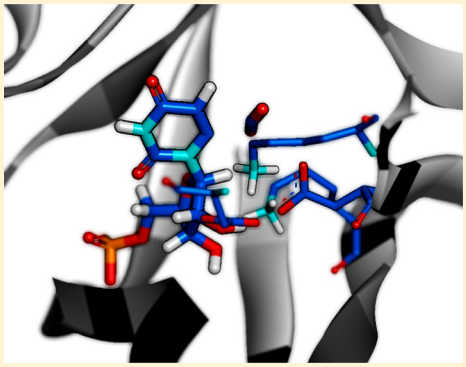

Orotidine 5′-monophosphate (OMP) decarboxylase (ODCase) catalyzes the decarboxylation of OMP to uridine 5′-monophosphate (UMP) (Scheme 1).[1] ODCase catalyzes the crucial final step in the pyrimidine biosynthetic pathway and presents a significant target in the development of antimalaria and cancer drugs.[2] Interestingly, ODCase is one of the most proficient enzymes known, enhancing the rate of spontaneous substrate decarboxylation by more than 17 orders of magnitude.[3−5] Indeed, the nonenzymatic rate constant extrapolated to 25 °C is $\sim 10^{-16}$ s^{-1}, corresponding to a half-life of 78 million years, while the ODCase catalyzed reaction has a turnover rate of 39 s^{-1}.[3]

Scheme 1. Decarboxylation of OMP by ODCase

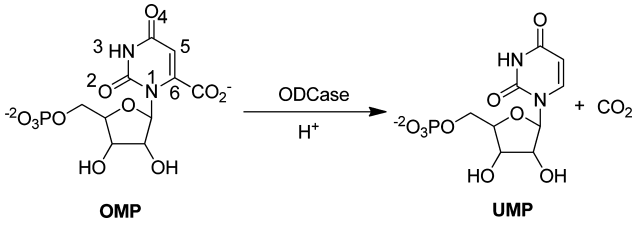

The catalytic mechanism of ODC has been subject to numerous investigations by both experimental[6−16] and theoretical[8,17−24] means. Several mechanisms have been proposed in the past decades, but a consensus has yet to emerge.[6,14−16,25] Beak and Siegel[9] suggested a mechanism in which the O2 carbonyl oxygen of the orotic acid moiety is protonated, necessitating formation of a ylide with a positively charged N1 during catalysis. The validity of this mechanism was questioned by ^{15}N kinetic isotope effect (KIE) experiments that showed no change in the bond order of N1 during the course of the reaction.[16] Moreover, no correctly positioned active site acid is present in the active site.[12,26] Lee and Houk suggested that the decarboxylation is accompanied by protonation at the O4 position rather than O2 based on model gas-phase computational studies.[22] This conclusion was further supported by DFT calculations due to Singleton at el.[27] Silverman and Groziak suggested a mechanism that involves a Michael addition of an active site nucleophile at the C5 position,[28,29] whereas Kollman and co-workers suggested that protonation at C5 could catalyze decarboxylation.[30] These mechanisms were ruled out by Acheson and co-workers who demonstrated a lack of secondary deuterium isotope effect for the C5 hydrogen.[7]

Recent KIE studies of Cleland and co-workers support the direct decarboxylation mechanism involving an anionic intermediate.[14,31] In addition, multiple isotope effect experi-

Received: February 14, 2013
Revised: May 21, 2013
Published: May 21, 2013

dx.doi.org/10.1021/bi400190v | *Biochemistry* 2013, 52, 4382−4390

ments were employed to determine whether protonation occurs in concert with decarboxylation for the ODCase reaction.[32] Therein the ^{13}C isotope effects did not increase when the aqueous solvent for the reaction was replaced with D_2O, showing that no protonation occurs as the C−C bond is cleaved, pointing to a stepwise mechanism. The stepwise decarboxylation followed by protonation by an active site Lys residue[33] has received accruing support by a series of NMR studies by Richard and co-workers.[31,34−36]

The direct decarboxylation followed by C6-protonation mechanism has gained acceptance in recent years based on a series of hybrid quantum mechanics−molecular mechanics (QM/MM) studies. The pioneering QM/MM work of Gao and co-workers suggested a direct decarboxylation mechanism, and excellent agreement with experimental kinetic data was obtained, although the question of proton transfer was not addressed.[8] Warshel and co-workers also sided with a direct decarboxylation mechanism followed by proton transfer, although the details of the proton transfer were not studied in the enzyme.[21] Surprisingly, more recent studies employing fairly accurate density function theory (DFT) QM methods obtained poor agreement with experimental kinetic data, with barriers considerably higher than those observed.[17,19,30] Raugei et al. also suggested a direct decarboxylation mechanism using DFT based Car−Parrinello/MM simulations, although the computed activation free energy barrier was significantly too high, and the question of C6-protonation was not rigorously addressed.[19] Interestingly, Houk and co-workers dismissed the direct decarboxylation mechanism based on the disagreement between their predicted and the experimentally observed kinetics, although an alternative mechanism was not presented.[17,37] A more recent DFT based QM/MM study of Yang and co-workers suggested that earlier failures to obtain reasonable reaction free energy barriers were due to the incorrect modeling of the enzyme system.[18] Indeed, this study presented a reaction free energy barrier in excellent agreement with experiment, although the proton transfer step was not explicitly monitored in this work.

In this paper, we present a detailed study of the decarboxylation reaction of OMP and 5-fluoro-OMP in the enzyme *Methanobacterium thermoautotrophicum* ODCase (*Mt*ODCase). The potential energy surface is described by a hybrid QM/MM potential, where the QM subsystem is treated by the semiempirical Austin model 1 (AM1) formalism,[38] which has been shown to give excellent results for decarboxylation reactions,[8,39−42] as well as for proton transfers involving Lys residues.[43,44] We derive a combined reaction progress coordinate based on three geometric metrics: the decarboxylation reaction coordinate, the rehybridization of the carboxylate leaving group, and the proton transfer coordinate from Lys72 to the C6 position of OMP. KIEs are computed employing a coupled free energy mass perturbation and umbrella sampling simulation technique based on Feynman centroid path integral calculations (PI-FEP/UM).[45] Thus, both the electronic structure of the reacting system and the nuclear dynamics are treated quantum mechanically. This combined approach has been successfully employed in a series of studies of chemical reactions in solution and in enzymes.[43,45−48]

1. METHODOLOGY

QM/MM Simulations of *Mt*ODCase. *Construction of the Michaelis Complex.* The active form of ODCase is a dimer with two active sites at the interface between the two monomers. Four residues in the active site were discovered to be important for catalytic activity. These residues include two Lys and one Asp from one monomer and one Asp residue from the other monomer.[8,12,49] Mutation of any of the four residues leads to partial or even complete loss of activity and also to reduction of substrate affinity.[14,50] Additionally, the phosphate and ribose group of the substrate (OMP) have been shown to contribute to binding and catalysis.[51−56] Numerous X-ray structures of native ODCase from different species and complexes with different inhibitors were solved in the past decade.[8,12,13,49,57,58] We chose to focus on the structure of *Mt*ODCase complexed with the inhibitor 6-hydroxy-OMP (BMP) at 1.4 Å.[26]

The crystal structure of the *Mt*ODCase dimer with the BMP inhibitor (PDB code 3LTP)[26] was used to construct the initial configuration for the present study. The X-ray crystal structure contains 218 amino acid residues in monomer A and 217 amino acid residues in monomer B, 142 crystallographic waters, and the BMP inhibitor.[26] The BMP inhibitor was modified to OMP in each monomer. The missing crystallographic amino acid residues 1−7 and 226−228 were added to monomer A and residues 1−8 and 226−228 were added to monomer B, using Discovery Studio 3.5 (Accelrys Inc.), prior to commencing the simulations. The residues were added in an extended conformation and subjected to geometry minimization and molecular dynamics (MD) simulations while the remainder of the enzyme was kept fixed. During these steps distance restraints were employed between Met1 and Met9 (approximately 8−9 Å) to hasten folding of the N-terminus during the minimization and dynamics. One BMP bound water molecule was deleted based on the suggestion of Hu et al.[18]

The protonation states of all ionizable residues were set corresponding to pH 7.[26] The hydrogen bonding patterns of the ionizable residues with the surrounding environment were visually inspected to verify that the protonation states are reasonable. The coordinates of hydrogen atoms of the protein and water were determined using the HBUILD facility in the program CHARMM.[59,60] The possible protonation states of His residues (protonated on Nε or Nδ or doubly protonated form) were determined by examination of the hydrogen bonding interactions. Peripheral/surface His residues were assumed to be positively charged. The resulting negatively charged enzyme (−20) has dimensions of approximately 64 × 59 × 66 Å^3. To this system we added 20 sodium ions in random positions outside the protein to obtain a net-neutral system.[61] Subsequently, the protein, ligands, crystal waters, and counterions were embedded in a water box as detailed below.

Hybrid QM/MM Potential Energy Surface. The hydride transfer reaction in ODCase was described using a hybrid QM/MM potential energy surface (PES).

$$\hat{H} = \hat{H}_{QM} + \hat{H}_{MM} + \hat{H}_{QM/MM} \quad (1)$$

The system was partitioned into a QM region consisting of 44 atoms and a MM region containing the rest of the system (Figure 1). The QM subsystem includes 26 atoms from the OMP substrate and 16 atoms from the Lys72 protein residue. Additionally, two hydrogen link atoms were introduced along the covalent bonds crossing the boundary between the QM and the MM regions, to satisfy the valence requirements of the QM fragments.

The QM region was treated by the AM1 Hamiltonian.[38] AM1 yields excellent results for model decarboxylation and

dx.doi.org/10.1021/bi400190v | *Biochemistry* 2013, 52, 4382−4390

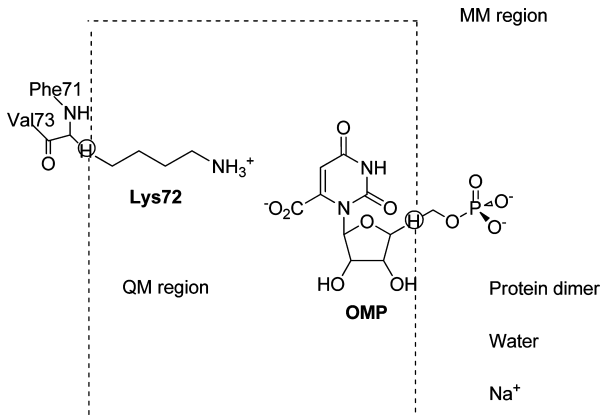

Figure 1. QM/MM partitioning scheme. The dashed line divides between the QM and MM regions.

proton transfer reactions involving amines[8,39−44] (see Tables S1 and S2 in Supporting Information). The effect of introducing a link atom on the current reaction was estimated by comparing the decarboxylation potential energy surface of OMP treated within a QM/MM framework with a link atom and OMP treated as fully QM. The results are nearly identical and demonstrate that the link atom approach is valid for this reaction (Figure S1). The all-atom CHARMM22/27 force field[62,63] with grid-based energy correction maps (CMAP)[64] for peptide dihedral angles was employed to treat the entire protein, the substrate, and the ions. The water molecules were represented by the three-point charge TIP3P model.[65] QM/MM interactions were treated by electrostatic embedding, wherein the MM partial atomic charges are included in the one-electron Hamiltonian.

Free Energy Simulations: General Approach.[45] We follow a two-step procedure in which we first carry out Newtonian MD simulations to determine the classical mechanical potential of mean force (PMF) along the reaction coordinate for the decarboxylation reaction in the fully solvated enzyme. Subsequently, atoms directly involved in the decarboxylation reaction are quantized via path-integral (PI) simulations. To this end, configurations sampled in the classical MD simulations are used as a configurational basin for the quantum simulations. This double (quantum and classical) averaging scheme is formally exact[45,66−68] and yields the QM-PMF as a function of the centroid reaction path.[69,70] In PI-FEP/UM, the ratio of the quantum partition functions for different isotopes, which yields the KIE, is obtained by free energy perturbation from a light isotope mass into a heavier one within the same centroid PI simulation.[45] This strategy avoids computing the difference between two free energy barriers, which have greater fluctuations than the difference itself for the two isotopic reactions.[45,47]

MD Simulations. MD simulations were conducted under periodic boundary conditions (PBC), with Ewald summation for electrostatic interactions.[71] The solute was soaked in a pre-equilibrated 81 × 81 × 81 Å^3 cubic box of 17 701 water molecules, with its longest axis lying along the space diagonal of the box to ensure that all protein atoms are at least 10 Å away from the edges of the box. The final model contained 52 677 atoms. For van der Waals and electrostatic interactions, a 13.0 Å group-based cutoff was used. The Ewald method was employed for reciprocal space summations between MM sites as well as for the QM/MM interactions using a 80 × 80 × 80 FFT grid.[71] The κ value was set to 0.340 Å^{-1}.

All water molecules were relaxed using the adopted basis set Newton−Raphson (ABNR) minimization method (30 steps), while the crystal water oxygens were harmonically restrained to their original positions. This was followed by a 100 ps MD equilibration of the water molecules, which were thereafter minimized again (30 steps ABNR). Subsequently, all atoms were subjected to minimization in a stepwise fashion to remove close contacts in the initial protein−ligand−solvent system: (a) The substrate was first minimized (30 step ABNR) while placing harmonic restraints on heavy atoms and keeping the rest of the system fixed. The restraints were gradually decreased to zero, while the substrate was further minimized (5 × 30 steps ABNR). (b) The water molecules and protein molecules were minimized (this time the substrate was held fixed) while the harmonic restraints on the water and protein heavy atoms were gradually reduced (4 × 10 steps ABNR). (c) Finally, the entire system was minimized (30 steps ABNR) without any restraints.

The isothermal−isobaric ensemble (NPT) was employed at 1 atm and 298 K using the extended system pressure/temperature (CPT) algorithm of Andersen[72] with an effective mass of 500 amu and the Hoover thermostat[73] with an effective mass of 1000 kcal mol^{-1} ps^{-2}. The SHAKE algorithm[74] was applied to constrain all MM bonds involving hydrogen atoms. The system was gradually heated up from 48 to 298 K during five sessions of 5 ps for a total of 25 ps and thereafter equilibrated at the target temperature (298 K) over the course of 1 ns at the MM level of theory. Finally, the system was equilibrated during the course of an additional 200 ps using the QM(AM1)/MM potential.

Nuclear Overhauser effect (NOE) harmonic restraints were added to distances between donors and acceptors of selected hydrogen bonds within the protein during early stages of the equilibration. All restraints were removed 100 ps prior to commencing the production phase.

Potential of Mean Force. The classical−mechanical potential of mean force (CM-PMF) was determined using the umbrella sampling technique in order to sample the high-energy regions of the PES.[75] The reaction coordinate (ζ) was defined as a collective reaction coordinate.[76] This collective coordinate is composed of three reaction coordinates (Figure 2). The first reaction coordinate is defined as the distance between the carboxyl carbon (C) and the C6 atom involved in the covalent bond to be cleaved during the decarboxylation reaction:

$$\zeta_{\mathrm{decarb}} = R(\mathrm{C6{-}C}) \tag{2}$$

The second reaction coordinate describes the hybridization state, χ, of the carboxyl carbon atom (C), namely, defining the ratio of the p vs s atomic orbital contributions to the hybrid orbital:

$$\zeta_{\mathrm{rehyb}} = \chi(\mathrm{C}) \tag{3}$$

The evaluation of the hybridization state relies on the model formulated by Pu et al.,[77] according to which the hybridization state can be linearly correlated with L, the distance from the central carbon atom to the line or plane, determined by the positions of its substituents, in the form $\chi(\mathrm{C}) = 1 + 2L$ for the leaving C carbon.

Taking advantage of this definition, we have

$$\zeta_{\mathrm{rehyb}} = 1 + 2L \tag{4}$$

dx.doi.org/10.1021/bi400190v | *Biochemistry* 2013, 52, 4382−4390

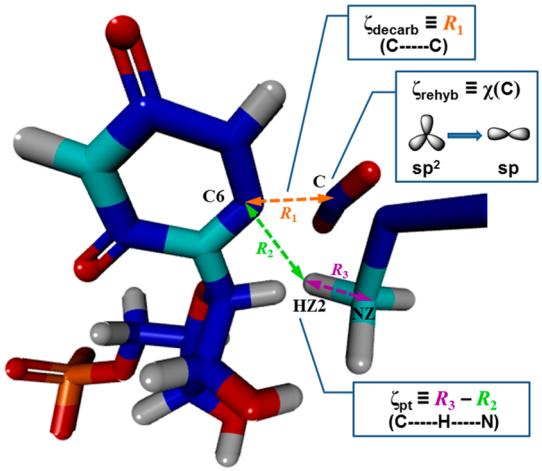

Figure 2. Depiction of the three reaction coordinates employed in the simulations of ODCase.

Specifically, in the reactant state (RS) of the ODCase catalyzed reaction, the carboxyl carbon adopts an approximate sp^2 hybridization, which corresponds to $\chi(C) = 2$ and $L = {}^1/_2$ Å. Accordingly, the upper boundary of ζ_{rehyb} in the RS has a theoretical value of 2 Å, while the product state (PS), where the sp-hybridized carbon dioxide is ultimately formed, is characterized by linear geometry of C, i.e., $\chi(C) = 1$ and $L = 0$ Å, resulting in lower limit of 1 Å.

Finally, the third reaction coordinate describes the proton transfer from Lys72 to the C6 carbon of OMP and is defined geometrically as the difference between the lengths of the breaking ($HZ2{-}NZ_{Lys72}$) and forming ($C6_{OMP}{-}HZ2$) bonds:

$$\zeta_{pt} = R(HZ2{-}NZ) - R(C6{-}HZ2) \quad (5)$$

The PMF is described as a function of these three reaction coordinates, and a collective reaction coordinate is defined as the minimum free energy path in the multidimensional reaction coordinate space. Practically, this path is obtained using the string method.[76,78] A total of 16 discrete regions along the reaction coordinate ("windows") were defined with spacing of 0.05−0.20 Å. Each simulation was performed with the addition of a biasing potential to the decarboxylation coordinate (roughly the negative of the computed PMF) and a harmonic restraint centered in each window for the decarboxylation coordinate and the proton transfer coordinate. The harmonic force constants, k, ranged between 5.0 and 80.0 kcal·mol^{-1}·Å^{-2} [$E_{harm} = k(\zeta - \zeta_{ref})^2$]. Each window was equilibrated for 75 ps, followed by 175 ps production simulations that collected the probability densities of configurations (ρ) along the reaction coordinates (ζ_i) and sorted them into bins of width 0.01−0.04 Å. The velocities and positions of the last configuration generated in each window were used to initiate the next window. The PMF curve was obtained using a multidimensional version of the weighted histogram analysis method (WHAM).[76,79] To ensure convergence of the PMF, the simulations were run until the difference between sequential PMF profiles was less than ±1 kcal/mol.

Quantum Monte Carlo Simulations and Kinetic Isotope Effects. The QM-PMF was obtained using a double averaging procedure by centroid PI simulations on configurations saved during the umbrella sampling simulations.[45,67,80] In essence, the centroid PI simulations yield the free energy difference between the classical mechanical and the quantum mechanical PMFs.[45,67,80]

The PI-FEP/UM method was used to compute KIE.[45] The method is based on quantum transition state theory and uses the bisection or staging sampling algorithms coupled with a mass-perturbation scheme to compute the KIEs directly.[45] The PI simulations were performed for each isotope (^{12}C, ^{13}C, ^{14}N, ^{15}N, ^{16}O, ^{18}O) for the decarboxylation reaction.

Specifically, to evaluate the KIEs, the centroid PI simulations were carried out for the light isotopic reaction, and the ratio of the partition functions between two isotopic reactions was determined by free energy perturbation theory from the light mass into the heavier one.[45] For the decarboxylation reaction, the isotope labeled atom was quantized in addition to three neighboring atoms. Each quantized particle was represented by paths discretized into 32 beads. We used the staging sampling technique[80,81] in all centroid PI simulations, sampling 10 free-particle configurations for each of 20 800 classical configurations in the RS and transition state (TS), yielding a total of 208 000 path-integral sampling steps.

2. RESULTS AND DISCUSSION

Reaction Mechanism in ODCase. Multidimensional umbrella sampling simulations were performed to obtain the free energy reaction profile for the ODCase catalyzed decarboxylation. This multidimensional strategy provides insight into the proton transfer and change in hybridization during the catalytic reaction. Two- and three-dimensional free energy surfaces are presented in Figure 3.

In Figure 3A we show the free energy as a function of the decarboxylation coordinate and the proton transfer coordinate while averaging the contributions of the rehybridization coordinate. This figure reflects the classical mechanical PMF (CM-PMF) for the ODCase decarboxylation reaction obtained from free energy MD simulations, using the QM(AM1)/MM Hamiltonian. The free energy barrier predicted by the corresponding PMF is $\Delta G^{\ddagger} = 15.7$ kcal/mol. The TS is located at $\zeta_{decarb} \approx 2.1$ Å and $\zeta_{pt} \approx -1.65$ Å prior to the onset of the proton transfer (Figure 4). Nonetheless, inspection of the minimum free energy path reveals that the formation of an ion pair between Lys72 and C6 of OMP and the decarboxylation step are coupled. A tight ion pair between Lys72 and the developing anion at C6 is progressively formed as CO_2 leaves. This Lys residue is held tightly in place by two strong hydrogen bonds to Asp70 and Asp75B (Figure 4), ready to donate a proton from one side of the pyrimidine plane while dissociation of CO_2 occurs on the opposite side of the pyrimidine plane. The proton is only transferred once the decarboxylation process is complete, and this step has no free energy barrier. The current results are consistent with experimental KIE[32,35] results pointing to a stepwise mechanism, wherein the proton transfer is not rate determining. Indeed, the current results are in remarkable agreement with the work of Richard and coworkers.[35] On the basis of product isotope effect experiments, they suggested that the rate-limiting step is the breakdown of OMP to form a C6 UMP carbanion intermediate and that the subsequent hydron transfer to C6 is faster than rotation of the Lys72 C−N bond. The current results support such a view on all accounts.

In addition to the role of Lys72 in facilitating reaction, several additional active site residues contribute to catalysis. In particular, Hu et al. suggested that Ser127 plays an important role in stabilizing the TS via hydrogen-bond interactions.[18] In

dx.doi.org/10.1021/bi400190v | Biochemistry 2013, 52, 4382−4390

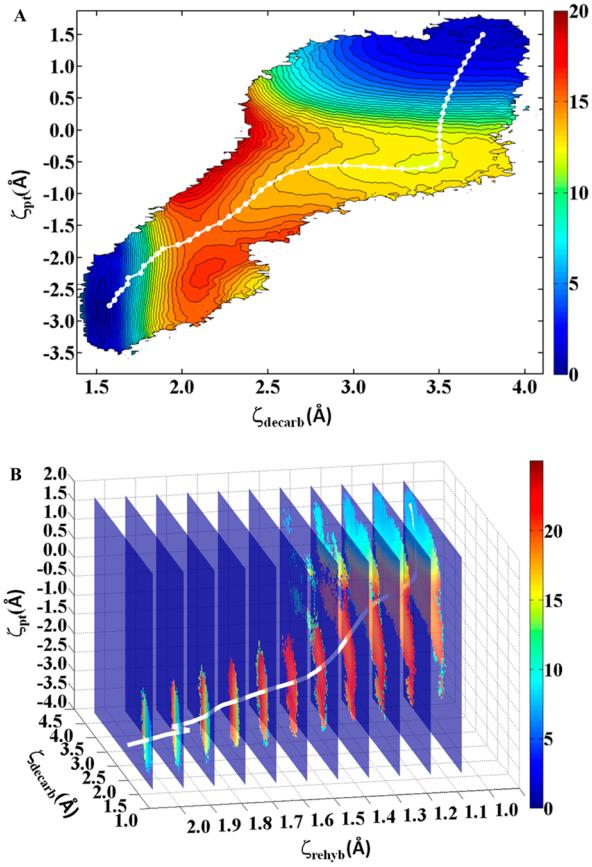

Figure 3. Classical (A) two- and (B) three-dimensional potential of mean force surfaces (kcal/mol) for the ODCase catalyzed decarboxylation reaction of OMP. Associated minimum free energy paths (white-colored curves in parts A and B) were obtained using the string method with 50 images.

Table S3 we present ensemble averaged distances between O4 in OMP and the Ser127 backbone amide nitrogen and between N3 in OMP and the Ser127 side chain. As is seen from the table, the H-bond distances are short and the substrate is held tightly in place during catalysis. These interactions provide further stabilization in addition to that of Lys72.

Figure 3B provides a multidimensional depiction of the classical mechanical free energy landscape for the ODCase catalyzed decarboxylation reaction. We employed a sampling scheme in which a biasing potential was imposed on the decarboxylation reaction coordinate and the proton reaction coordinate, while the rehybridization coordinates were used as a spectator coordinate. In this description, isosurfaces are drawn along ζ_{rehyb} spanning the entire reaction coordinate, and each surface represents a "slice" of the free energy surface.

Analysis of the figure shows that the change in hybridization of the CO_2 carbon occurs during the decarboxylation reaction. The starting value is $\zeta_{rehyb} \approx 2$ Å (RS). As the bond between C6 and CO_2 starts to break, the rehybridization decreases. At the TS, the value of the rehybridization coordinate is ∼1.5 Å and the value of decarboxylation coordinate is ∼2.2 Å. Thus, near the TS the decarboxylation coordinate and the rehybridization coordinate are synchronized. The rehybridization coordinate reaches its end value ($\zeta_{dehyb} \approx 1$ Å) at around $\zeta_{decarb} \approx 3.5$ Å and does not change during the proton transfer step. The reaction free energy is ∼1.2 kcal/mol, suggesting that the reaction could be reversible.[82−84] The reverse reaction would require a proton abstraction followed by electrophilic addition of CO_2 to the carbanion. The barrier for the latter of these two steps is 3.5 kcal/mol, suggesting that the decarboxylation reaction could be reversible.

The QM-PMF is obtained from Feynman PI calculations[45,66,68] in which the centroid positions of the discrete paths of quantized particles are used to specify the reaction coordinate.[45,69,70] By use of QM(AM1)/MM, inclusion of nuclear quantum effects (NQE) in the simulations[45] lowers the computed free energies of activation by 0.8 kcal/mol, yielding a quantum free energy of activation for the decarboxylation of 14.9 kcal/mol. Direct comparison with experiment is not possible, as product release is strongly rate limiting for this system.[58] Nonetheless, if an upper limit to the experimental free energy of activation is calculated from the phenomeno-

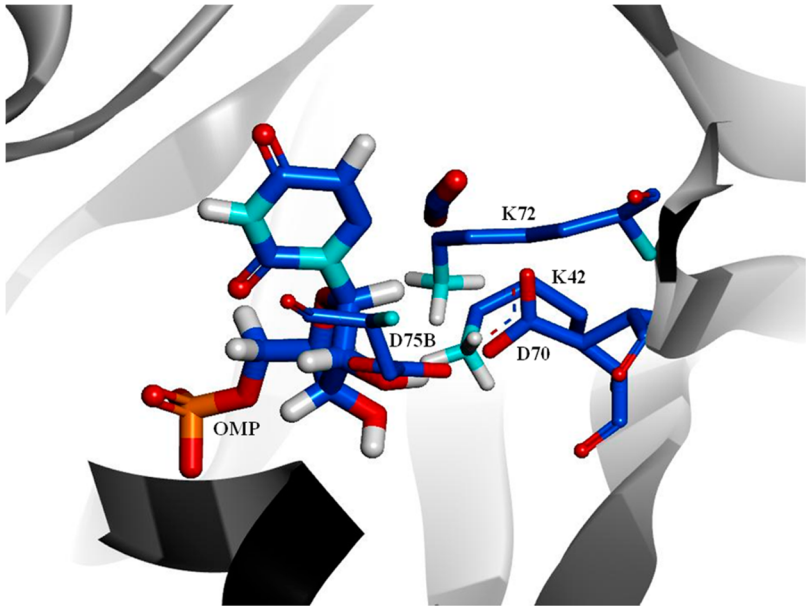

Figure 4. Snapshot of the transition state in the active site of ODCase obtained by QM(AM1)/MM molecular dynamics simulations.

dx.doi.org/10.1021/bi400190v | *Biochemistry* 2013, 52, 4382−4390

logical rate constant (k_{cat}) using transition state theory, a value of 16.6 kcal/mol is obtained[58] in good agreement with our result.

We also performed multidimensional umbrella sampling simulations to obtain the free energy reaction profile for the ODCase catalyzed decarboxylation of 5-fluoro-OMP. In Figure 5 we show the free energy as a function of the decarboxylation

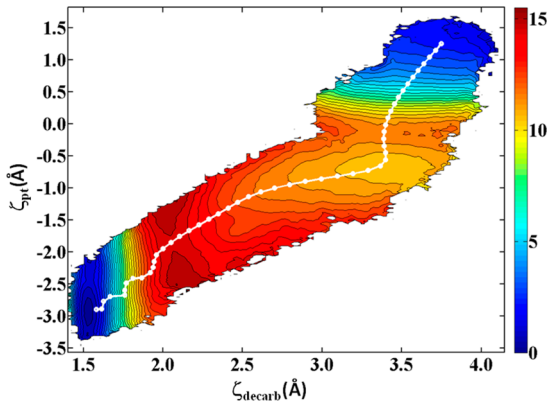

Figure 5. Classical two-dimensional potential of mean force surface (kcal/mol) for the ODCase catalyzed decarboxylation reaction of 5-fluoro-OMP. The associated minimum free energy path (white-colored) were obtained using the string method with 50 images.

coordinate and the proton transfer coordinate while averaging the contributions of the rehybridization coordinate. The free energy barrier predicted by the corresponding PMF is $\Delta G^{\ddagger}$ = 14.7 kcal/mol. The TS is located at $\zeta_{decarb} \approx 2.1$ Å and $\zeta_{pt} \approx -2.0$ Å prior to the onset of the proton transfer. Comparison of these results to the free energy profile of OMP shows a lower energy barrier (by approximately −1.0 kcal/mol) and slightly earlier TS. We also observed that 5-fluoro-OMP exhibits a weaker ion pair between Lys72 and the developing anion at C6 in comparison to OMP ($\zeta_{pt} \approx -1.65$ Å for the TS of OMP compared to $\zeta_{pt} \approx -2.0$ Å for the TS of 5-fluoro-OMP). A slight barrier to protonation of the carbanion is also observed. These changes may be ascribed to an inductive effect of the fluorine, which stabilizes the carbanion intermediate by electron withdrawal and produces a reaction with a lower barrier and an earlier transition state. The reverse electrophilic addition of CO_2 to the carbanion has a free energy barrier of 4.4 kcal/mol, which is slightly higher than for OMP. As is the case for OMP, the results for 5-fluoro-OMP are in line with the conclusions of Richard and co-workers based on product isotope effects, which suggest that the reaction is stepwise, yet synchronous.

Inclusion of NQE in the simulations[45] lowers the computed free energy of activation for 5-fluoro-OMP by ∼0.7 kcal/mol, resulting in a quantum free energy of activation for the decarboxylation of 14.0 kcal/mol. This value is similar to that obtained from the experimental k_{cat} which yields a phenomenological activation free energy of 14.1 kcal/mol.[58] The effect of the 5-fluoro substitution from our simulations is thus 0.9 kcal/mol. This effect is somewhat lower than the 3.5 kcal/mol value estimated by Richard and co-workers.[85] The reason for the slight underestimation of the effect of the 5-fluoro substitution is possibly due to the AM1 method employed for the QM region in this work. Inspection of Table S2 reveals that AM1 underestimates the effect of the 5-fluoro substituent on C6 anion formation by 2.1 kcal/mol compared to the M06 DFT method.

Kinetic Isotope Effects. The KIEs for OMP were computed using a mass-perturbation-based PI approach as described in the methods section, and the results are summarized in Table 1. The computed intrinsic KIE for the

Table 1. Comparison between the Computed and Experimental Intrinsic Kinetic Isotope Effect Values for the Decarboxylation Reaction in ODCase at 298 K

	KIE	
	calcd	exptl
	OMP	
CO_2	1.050 ± 0.006	1.0494 ± 0.0006 [6,16]
N1	1.003 ± 0.005	1.0068 ± 0.0003 [16]
O2	0.998 ± 0.005	0.983 ± 0.001 [15]
O4	1.004 ± 0.007	
	5-Fluoro-OMP	
CO_2	1.047 ± 0.009	1.0356 ± 0.0001 [14]
N1	1.004 ± 0.006	
O2	0.998 ± 0.005	
O4	1.001 ± 0.005	

carboxyl group carbon is 1.050 ± 0.006, in good agreement with the experimental intrinsic KIE value of 1.0494 ± 0.0006.[6,16] The computed intrinsic KIE for the N1 position is 1.003 ± 0.005. This result is also in reasonable agreement with the experimental intrinsic KIE value of 1.0068 ± 0.0003.[16] The computed intrinsic KIE for the O2 position is 0.998 ± 0.005, and for the O4 position it is 1.004 ± 0.007. The O2 result is in good agreement with the experimental intrinsic KIE value of 0.983 ± 0.001.[15]

We also computed the KIEs for 5-fluoro-OMP using the methodology described above, and the results are summarized in Table 1. The computed intrinsic KIE for the carboxyl group carbon is 1.047 ± 0.009. This result is in good agreement with the experimental intrinsic KIE of value 1.0356 ± 0.0001.[14] The slightly lower KIE value of the fluorinated OMP supports the notion of an inductive effect of fluorine and of an earlier TS than that for OMP. The computed intrinsic KIE for the N1 position is 1.004 ± 0.006, while the computed intrinsic KIE for the O2 position is 0.998 ± 0.005 and for the O4 position is 1.001 ± 0.005.

In conclusion, the current free energy reaction profiles and KIE provide further support for a direct decarboxylation mechanism, followed by protonation by Lys72.

3. SUMMARY

In this article we present for the first time a complete free energy landscape for the ODCase catalyzed decarboxylation reaction, including the proton transfer step. Our results show that decarboxylation of OMP is the rate-determining step with a free energy barrier of 14.9 kcal/mol, in good agreement with the experimental upper estimate of 16.4 kcal/mol. The simulations suggest that although the decarboxylation and protonation steps are stepwise, the formation of an ion pair between the positively charged Lys72 and the developing anion at the C6 atom of OMP is tightly coupled to the decarboxylation step. We have also calculated the complete free energy landscape for the ODCase catalyzed decarboxylation reaction of 5-fluoro-OMP. Our results show that decarboxylation of 5-fluoro-OMP is the rate-determining step with a free energy barrier of 14.0 kcal/mol, in good agreement with the experimental upper estimate of 14.1 kcal/mol. The

dx.doi.org/10.1021/bi400190v | Biochemistry 2013, 52, 4382−4390

computed effect of the 5-fluoro substitution on the decarboxylation free energy barrier is thus 0.9 kcal/mol, slightly less than the 3.5 kcal/mol value predicted by experiment.[85] The simulation of 5-fluoro-OMP exhibits a weaker ion pair between Lys72 and the developing anion at C6 and an earlier transition state. These changes are caused by the inductive effect of fluorine, which stabilizes the carbanion intermediate. Computed kinetic isotope effects were found to be in good agreement with experiment and serve as further support for a direct decarboxylation mechanism.

■ ASSOCIATED CONTENT

Ⓢ Supporting Information

Energy results for model decarboxylation and proton transfer reactions in the gas phase and in water; coordinates of model molecules calculated using density functional theory and semiempirical methods. This material is available free of charge via the Internet at http://pubs.acs.org.

■ AUTHOR INFORMATION

Corresponding Author

*Phone: 972-3-5317392. E-mail: majort@biu.ac.il.

Funding

This work has been supported by the Israel Science Foundation.

Notes

The authors declare no competing financial interest.

■ REFERENCES

(1) Bell, J. B., and Jones, M. E. (1991) Purification and characterization of yeast orotidine 5′-monophosphate decarboxylase overexpressed from plasmid PGU2. *J. Biol. Chem. 266*, 12662−12667.

(2) Christopherson, R. I., Lyons, S. D., and Wilson, P. K. (2002) Inhibitors of de novo nucleotide biosynthesis as drugs. *Acc. Chem. Res. 35*, 961−971.

(3) Radzicka, A., and Wolfenden, R. (1995) A proficient enzyme. *Science 267*, 90−93.

(4) Miller, B. G., and Wolfenden, R. (2002) Catalytic proficiency: the unusual case of OMP decarboxylase. *Annu. Rev. Biochem. 71*, 847−885.

(5) Wolfenden, R., and Snider, M. J. (2001) The depth of chemical time and the power of enzymes as catalysts. *Acc. Chem. Res. 34*, 938−945.

(6) Smiley, J. A., Paneth, P., O'Leary, M. H., Bell, J. B., and Jones, M. E. (1991) Investigation of the enzymic mechanism of yeast orotidine-5′-monophosphate decarboxylase using carbon-13 kinetic isotope effects. *Biochemistry 30*, 6216−6223.

(7) Acheson, S. A., Bell, J. B., Jones, M. E., and Wolfenden, R. (1990) Orotidine-5′-monophosphate decarboxylase catalysis: kinetic isotope effects and the state of hybridization of a bound transition-state analog. *Biochemistry 29*, 3198−3202.

(8) Wu, N., Mo, Y., Gao, J., and Pai, E. F. (2000) Electrostatic stress in catalysis: structure and mechanism of the enzyme orotidine monophosphate decarboxylase. *Proc. Natl. Acad. Sci. U.S.A. 97*, 2017.

(9) Beak, P., and Siegel, B. (1976) Mechanism of decarboxylation of 1,3-dimethylorotic acid. A model for orotidine 5′-phosphate decarboxylase. *J. Am. Chem. Soc. 98*, 3601−3606.

(10) Cleland, W., and Kreevoy, M. M. (1994) Low-barrier hydrogen bonds and enzymic catalysis. *Science 264*, 1887−1890.

(11) Wu, W., Ley-han, A., Wong, F. M., Austin, T. J., and Miller, S. M. (1997) Decarboxylation of 1,3-dimethylorotic acid revisited: determining the role of N-1. *Bioorg. Med. Chem. Lett. 7*, 2623−2628.

(12) Miller, B. G., Hassell, A. M., Wolfenden, R., Milburn, M. V., and Short, S. A. (2000) Anatomy of a proficient enzyme: the structure of orotidine 5′-monophosphate decarboxylase in the presence and absence of a potential transition state analog. *Proc. Natl. Acad. Sci. U.S.A. 97*, 2011.

(13) Iiams, V., Desai, B. J., Fedorov, A. A., Fedorov, E. V., Almo, S. C., and Gerlt, J. A. (2011) Mechanism of the orotidine 5′-monophosphate decarboxylase-catalyzed reaction: importance of residues in the orotate binding site. *Biochemistry 50*, 8497−8507.

(14) Van Vleet, J. L., Reinhardt, L. A., Miller, B. G., Sievers, A., and Cleland, W. W. (2008) Carbon isotope effect study on orotidine 5′-monophosphate decarboxylase: support for an anionic intermediate. *Biochemistry 47*, 798−803.

(15) Wepukhulu, W. O., Smiley, V. L., Vemulapalli, B., Smiley, J. A., Phillips, L. M., and Lee, J. K. (2008) A substantial oxygen isotope effect at O2 in the OMP decarboxylase reaction: mechanistic implications. *Org. Biomol. Chem. 6*, 4533−4541.

(16) Rishavy, M. A., and Cleland, W. (2000) Determination of the mechanism of orotidine 5′-monophosphate decarboxylase by isotope effects. *Biochemistry 39*, 4569−4574.

(17) Stanton, C. L., Kuo, I. F. W., Mundy, C. J., Laino, T., and Houk, K. N. (2007) QM/MM metadynamics study of the direct decarboxylation mechanism for orotidine-5′-monophosphate decarboxylase using two different QM regions: acceleration too small to explain rate of enzyme catalysis. *J. Phys. Chem. B 111*, 12573−12581.

(18) Hu, H., Boone, A., and Yang, W. T. (2008) Mechanism of OMP decarboxylation in orotidine 5′-monophosphate decarboxylase. *J. Am. Chem. Soc. 130*, 14493−14503.

(19) Raugei, S., Cascella, M., and Carloni, P. (2004) A proficient enzyme: insights on the mechanism of orotidine monophosphate decarboxylase from computer simulations. *J. Am. Chem. Soc. 126*, 15730−15737.

(20) Chen, D., Wang, J., Zhang, H., Mi, S., Zhang, G., Wang, Q., and Zeng, Q. (2009) Effect of water molecules on the decarboxylation of orotidine 5′-monophosphate catalyzed by orotidine 5′-monophosphate decarboxylase. *J. Mol. Struct.: THEOCHEM 897*, 139−144.

(21) Warshel, A., Štrajbl, M., Villà, J., and Florián, J. (2000) Remarkable rate enhancement of orotidine 5′-monophosphate decarboxylase is due to transition-state stabilization rather than to ground-state destabilization. *Biochemistry 39*, 14728−14738.

(22) Lee, J. K., and Houk, K. (1997) A proficient enzyme revisited: the predicted mechanism for orotidine monophosphate decarboxylase. *Science 276*, 942−945.

(23) Feng, W. Y., Austin, T. J., Chew, F., Gronert, S., and Wu, W. (2000) The mechanism of orotidine 5′-monophosphate decarboxylase: catalysis by destabilization of the substrate. *Biochemistry 39*, 1778−1783.

(24) Phillips, L. M., and Lee, J. K. (2001) Theoretical studies of mechanisms and kinetic isotope effects on the decarboxylation of orotic acid and derivatives. *J. Am. Chem. Soc. 123*, 12067−12073.

(25) Ehrlich, J. I., Hwang, C.-C., Cook, P. F., and Blanchard, J. S. (1999) Evidence for a stepwise mechanism of OMP decarboxylase. *J. Am. Chem. Soc. 121*, 6966−6967.

(26) Wood, B. M., Amyes, T. L., Fedorov, A. A., Fedorov, E. V., Shabila, A., Almo, S. C., Richard, J. P., and Gerlt, J. A. (2010) Conformational changes in orotidine 5′-monophosphate decarboxylase: "remote" residues that stabilize the active conformation. *Biochemistry 49*, 3514−3516.

(27) Singleton, D. A., Merrigan, S. R., Kim, B. J., Beak, P., Phillips, L. M., and Lee, J. K. (2000) ^{13}C kinetic isotope effects and the mechanism of the uncatalyzed decarboxylation of orotic acid. *J. Am. Chem. Soc. 122*, 3296−3300.

(28) Silverman, R. B., and Groziak, M. P. (1982) Model chemistry for a covalent mechanism of action of orotidine 5′-phosphate decarboxylase. *J. Am. Chem. Soc. 104*, 6434−6439.

(29) Bello, A. M., Poduch, E., Fujihashi, M., Amani, M., Li, Y., Crandall, I., Hui, R., Lee, P. I., Kain, K. C., Pai, E. F., and Kotra, L. P. (2007) A potent, covalent inhibitor of orotidine 5′-monophosphate decarboxylase with antimalarial activity. *J. Med. Chem. 50*, 915−921.

(30) Lee, T.-S., Chong, L. T., Chodera, J. D., and Kollman, P. A. (2001) An alternative explanation for the catalytic proficiency of

orotidine 5′-phosphate decarboxylase. *J. Am. Chem. Soc. 123*, 12837−12848.
(31) Toth, K., Amyes, T. L., Wood, B. M., Chan, K., Gerlt, J. A., and Richard, J. P. (2007) Product deuterium isotope effect for orotidine 5′-monophosphate decarboxylase: evidence for the existence of a short-lived carbanion intermediate. *J. Am. Chem. Soc. 129*, 12946−12947.
(32) Ehrlich, J. I., Hwang, C.-C., Cook, P. F., and Blanchard, J. S. (1999) Evidence for a stepwise mechanism of OMP decarboxylase. *J. Am. Chem. Soc. 121*, 6966−6967.
(33) Smiley, J. A., and Jones, M. E. (1992) A Unique Catalytic and Inhibitor-Binding Role for LYS93 of Yeast Orotidylate Decarboxylate. *Biochemistry 31*, 12162−12168.
(34) Amyes, T. L., Wood, B. M., Chan, K., Gerlt, J. A., and Richard, J. P. (2008) Formation and stability of a vinyl carbanion at the active site of orotidine 5′-monophosphate decarboxylase: pK_a of the C-6 proton of enzyme-bound UMP. *J. Am. Chem. Soc. 130*, 1574−1575.
(35) Toth, K., Amyes, T. L., Wood, B. M., Chan, K., Gerlt, J. A., and Richard, J. P. (2010) Product deuterium isotope effects for orotidine 5′-monophosphate decarboxylase: effect of changing substrate and enzyme structure on the partitioning of the vinyl carbanion reaction intermediate. *J. Am. Chem. Soc. 132*, 7018−7024.
(36) Tsang, W.-Y., Wood, B. M., Wong, F. M., Wu, W., Gerlt, J. A., Amyes, T. L., and Richard, J. P. (2012) Proton transfer from C-6 of uridine 5′-monophosphate catalyzed by orotidine 5′-monophosphate decarboxylase: formation and stability of a vinyl carbanion intermediate and the effect of a 5-fluoro substituent. *J. Am. Chem. Soc. 134*, 14580−14594.
(37) Nosrati, G. R., and Houk, K. N. (2012) Using catalytic atom maps to predict the catalytic functions present in enzyme active sites. *Biochemistry 51*, 7321−7329.
(38) Dewar, M. J. S., Zoebisch, E. G., Healy, E. F., and Stewart, J. J. P. (1985) Development and use of quantum mechanical molecular models. 76. AM1: a new general purpose quantum mechanical molecular model. *J. Am. Chem. Soc. 107*, 3902−3909.
(39) Gao, J. (1995) An automated procedure for simulating chemical reactions in solution. Application to the decarboxylation of 3-carboxybenzisoxazole in water. *J. Am. Chem. Soc. 117*, 8600−8607.
(40) Gao, J. (2003) Catalysis by enzyme conformational change as illustrated by orotidine 5′-monophosphate decarboxylase. *Curr. Opin. Struct. Biol. 13*, 184−192.
(41) Lill, S. O. N., Gao, J., and Waldrop, G. L. (2008) Molecular dynamics simulations of biotin carboxylase. *J. Phys. Chem. B 112*, 3149−3156.
(42) Sicinska, D., Truhlar, D. G., and Paneth, P. (2005) Dependence of transition state structure on substrate: the intrinsic C-13 kinetic isotope effect is different for physiological and slow substrates of the ornithine decarboxylase reaction because of different hydrogen bonding structures. *J. Am. Chem. Soc. 127*, 5414−5422.
(43) Major, D. T., and Gao, J. L. (2006) A combined quantum mechanical and molecular mechanical study of the reaction mechanism and alpha-amino acidity in alanine racemase. *J. Am. Chem. Soc. 128*, 16345−16357.
(44) Major, D. T., Nam, K., and Gao, J. L. (2006) Transition state stabilization and alpha-amino carbon acidity in alanine racemase. *J. Am. Chem. Soc. 128*, 8114−8115.
(45) Major, D. T., and Gao, J. L. (2007) An integrated path integral and free-energy perturbation-umbrella sampling method for computing kinetic isotope effects of chemical reactions in solution and in enzymes. *J. Chem. Theory Comput. 3*, 949−960.
(46) Major, D. T., York, D. M., and Gao, J. L. (2005) Solvent polarization and kinetic isotope effects in nitroethane deprotonation and implications to the nitroalkane oxidase reaction. *J. Am. Chem. Soc. 127*, 16374−16375.
(47) Gao, J. L., Wong, K. Y., and Major, D. T. (2008) Combined QM/MM and path integral simulations of kinetic isotope effects in the proton transfer reaction between nitroethane and acetate ion in water. *J. Comput. Chem. 29*, 514−522.
(48) Major, D. T., Heroux, A., Orville, A. M., Valley, M. P., Fitzpatrick, P. F., and Gao, J. (2009) Differential quantum tunneling contributions in nitroalkane oxidase catalyzed and the uncatalyzed proton transfer reaction. *Proc. Natl. Acad. Sci. U.S.A. 106*, 20734−20739.
(49) Appleby, T. C., Kinsland, C., Begley, T. P., and Ealick, S. E. (2000) The crystal structure and mechanism of orotidine 5′-monophosphate decarboxylase. *Proc. Natl. Acad. Sci. U.S.A. 97*, 2005.
(50) Miller, B. G., Snider, M. J., Wolfenden, R., and Short, S. A. (2001) Dissecting a charged network at the active site of orotidine-5′-phosphate decarboxylase. *J. Biol. Chem. 276*, 15174.
(51) Amyes, T. L., Ming, S. A., Goldman, L. M., Wood, B. M., Desai, B. J., Gerlt, J. A., and Richard, J. P. (2012) Orotidine 5′-monophosphate decarboxylase: transition state stabilization from remote protein−phosphodianion interactions. *Biochemistry 51*, 4630−4632.
(52) Desai, B. J., Wood, B. M., Fedorov, A. A., Fedorov, E. V., Goryanova, B., Amyes, T. L., Richard, J. P., Almo, S. C., and Gerlt, J. A. (2012) Conformational changes in orotidine 5′-monophosphate decarboxylase: a structure-based explanation for how the 5′-phosphate group activates the enzyme. *Biochemistry 51*, 8665−8678.
(53) Goryanova, B., Amyes, T. L., Gerlt, J. A., and Richard, J. P. (2011) OMP decarboxylase: phosphodianion binding energy is used to stabilize a vinyl carbanion intermediate. *J. Am. Chem. Soc. 133*, 6545−6548.
(54) Miller, B. G., Butterfoss, G. L., Short, S. A., and Wolfenden, R. (2001) Role of enzyme−ribofuranosyl contacts in the ground state and transition state for orotidine 5′-phosphate decarboxylase: a role for substrate destabilization? *Biochemistry 40*, 6227−6232.
(55) Amyes, T. L., Richard, J. P., and Tait, J. J. (2005) Activation of orotidine 5′-monophosphate decarboxylase by phosphite dianion: the whole substrate is the sum of two parts. *J. Am. Chem. Soc. 127*, 15708−15709.
(56) Sievers, A., and Wolfenden, R. (2005) The effective molarity of the substrate phosphoryl group in the transition state for yeast OMP decarboxylase. *Bioorg. Chem. 33*, 45−52.
(57) Harris, P., Navarro Poulsen, J.-C., Jensen, K. F., and Larsen, S. (2000) Structural basis for the catalytic mechanism of a proficient enzyme: orotidine 5′-monophosphate decarboxylase. *Biochemistry 39*, 4217−4224.
(58) Chan, K. K., Wood, B. M., Fedorov, A. A., Fedorov, E. V., Imker, H. J., Amyes, T. L., Richard, J. P., Almo, S. C., and Gerlt, J. A. (2009) Mechanism of the orotidine 5′-monophosphate decarboxylase-catalyzed reaction: evidence for substrate destabilization. *Biochemistry 48*, 5518−5531.
(59) Brooks, B. R., Bruccoleri, R. E., Olafson, B. D., States, D. J., Swaminathan, S., and Karplus, M. (1983) CHARMM: a program for macromolecular energy, minimization, and dynamics calculations. *J. Comput. Chem. 4*, 187−217.
(60) Brooks, B. R., Brooks, C. L., III, Mackerell, A. D., Jr., Nilsson, L., Petrella, R. J., Roux, B., Won, Y., Archontis, G., Bartels, C., Boresch, S., Caflisch, A., Caves, L., Cui, Q., Dinner, A. R., Feig, M., Fischer, S., Gao, J., Hodoscek, M., Im, W., Kuczera, K., Lazaridis, T., Ma, J., Ovchinnikov, V., Paci, E., Pastor, R. W., Post, C. B., Pu, J. Z., Schaefer, M., Tidor, B., Venable, R. M., Woodcock, H. L., Wu, X., Yang, W., York, D. M., and Karplus, M. (2009) CHARMM: the biomolecular simulation program. *J. Comput. Chem. 30*, 1545−1614.
(61) Allen, M. P., and Tildesley, D. J. (1987) *Computer Simulation of Liquids*, pp 156−162, Oxford University Press, Oxford, U.K.
(62) MacKerell, A. D., Jr., Bashford, D., Bellott, Dunbrack, R. L., Evanseck, J. D., Field, M. J., Fischer, S., Gao, J., Guo, H., Ha, S., Joseph-McCarthy, D., Kuchnir, L., Kuczera, K., Lau, F. T. K., Mattos, C., Michnick, S., Ngo, T., Nguyen, D. T., Prodhom, B., Reiher, W. E., Roux, B., Schlenkrich, M., Smith, J. C., Stote, R., Straub, J., Watanabe, M., Wiorkiewicz-Kuczera, J., Yin, D., and Karplus, M. (1998) All-atom empirical potential for molecular modeling and dynamics studies of proteins. *J. Phys. Chem. B 102*, 3586−3616.
(63) MacKerell, A. D., Banavali, N., and Foloppe, N. (2000) Development and current status of the CHARMM force field for nucleic acids. *Biopolymers 56*, 257−265.

(64) MacKerell, A. D., Feig, M., and Brooks, C. L., III. (2004) Extending the treatment of backbone energetics in protein force fields: limitations of gas-phase quantum mechanics in reproducing protein conformational distributions in molecular dynamics simulations. *J. Comput. Chem. 25*, 1400−1415.
(65) Jorgensen, W. L., Chandrasekhar, J., Madura, J. D., Impey, R. W., and Klein, M. L. (1983) Comparison of simple potential functions for simulating liquid water. *J. Chem. Phys. 79*, 926−935.
(66) Major, D. T., Garcia-Viloca, M., and Gao, J. L. (2006) Path integral simulations of proton transfer reactions in aqueous solution using combined QM/MM potentials. *J. Chem. Theory Comput. 2*, 236−245.
(67) Hwang, J. K., Chu, Z. T., Yadav, A., and Warshel, A. (1991) Simulations of quantum mechanical corrections for rate constants of hydride-transfer reactions in enzymes and solutions. *J. Phys. Chem. 95*, 8445−8448.
(68) Major, D. T., and Gao, J. L. (2005) Implementation of the bisection sampling method in path integral simulations. *J. Mol. Graphics Modell. 24*, 121−127.
(69) Cao, J., and Voth, G. A. (1996) A unified framework for quantum activated rate processes. I. General theory. *J. Chem. Phys. 105*, 6856−6870.
(70) Gillan, M. J. (1987) Quantum simulation of hydrogen in metals. *Phys. Rev. Lett. 58*, 563.
(71) Nam, K., Gao, J., and York, D. M. (2005) An efficient linear-scaling ewald method for long-range electrostatic interactions in combined QM/MM calculations. *J. Chem. Theory Comput. 1*, 2−13.
(72) Andersen, H. C. (1980) Molecular dynamics simulations at constant pressure and/or temperature. *J. Chem. Phys. 72*, 2384−2393.
(73) Hoover, W. G. (1985) Canonical dynamics: equilibrium phase-space distributions. *Phys. Rev. A: At., Mol., Opt. Phys. 31*, 1695.
(74) Ryckaert, J.-P., Ciccotti, G., and Berendsen, H. J. C. (1977) Numerical integration of the Cartesian equations of motion of a system with constraints: molecular dynamics of *n*-alkanes. *J. Comput. Phys. 23*, 327−341.
(75) Torrie, G. M., and Valleau, J. P. (1977) Nonphysical sampling distributions in Monte Carlo free-energy estimation: umbrella sampling. *J. Comput. Phys. 23*, 187−199.
(76) Doron, D., Kohen, A., and Major, D. T. (2012) Collective reaction coordinate for hybrid quantum and molecular mechanics simulations: a case study of the hydride transfer in dihydrofolate reductase. *J. Chem. Theory Comput. 8*, 2484−2496.
(77) Pu, J., Ma, S., Garcia-Viloca, M., Gao, J., Truhlar, D. G., and Kohen, A. (2005) Nonperfect synchronization of reaction center rehybridization in the transition state of the hydride transfer catalyzed by dihydrofolate reductase. *J. Am. Chem. Soc. 127*, 14879−14886.
(78) E, W. N., Ren, W. Q., and Vanden-Eijnden, E. (2007) Simplified and improved string method for computing the minimum energy paths in barrier-crossing events. *J. Chem. Phys. 126*, 164103.
(79) Kumar, S., Rosenberg, J. M., Bouzida, D., Swendsen, R. H., and Kollman, P. A. (1992) The weighted histogram analysis method for free-energy calculations on biomolecules. I. The method. *J. Comput. Chem. 13*, 1011−1021.
(80) Sprik, M., Klein, M. L., and Chandler, D. (1985) Staging: a sampling technique for the Monte-Carlo evaluation of path-integrals. *Phys. Rev. B: Condens. Matter 31*, 4234−4244.
(81) Azuri, A., Engel, H., Doron, D., and Major, D. T. (2011) Path-integral calculations of nuclear quantum effects in model systems, small molecules, and enzymes via gradient based forward corrector algorithms. *J. Chem. Theory. Comput. 7*, 1273−1286.
(82) Mundle, S. O. C., Rathgeber, S., Lacrampe-Couloume, G., Sherwood Lollar, B., and Kluger, R. (2009) Internal return of carbon dioxide in decarboxylation: catalysis of separation and $^{12}C/^{13}C$ kinetic isotope effects. *J. Am. Chem. Soc. 131*, 11638−11639.
(83) Howe, G. W., Bielecki, M., and Kluger, R. (2012) Base-catalyzed decarboxylation of mandelylthiamin: direct formation of bicarbonate as an alternative to formation of CO_2. *J. Am. Chem. Soc. 134*, 20621−20623.
(84) Roca, M., Pascual-Ahuir, J.-L., and Tuñón, I. (2012) Reversibility and diffusion in mandelythiamin decarboxylation. Searching dynamical effects in decarboxylation reactions. *J. Am. Chem. Soc. 134*, 10509−10514.
(85) Goryanova, B., Spong, K., Amyes, T. L., and Richard, J. P. (2013) Catalysis by orotidine 5′-monophosphate decarboxylase: effect of 5-fluoro and 4′-substituents on the decarboxylation of two-part substrates. *Biochemistry 52*, 537−546.